Tracking the inflammatory response in stroke in vivo by sensing the enzyme myeloperoxidase

Michael O. Breckwoldt[a,b,1,2], John W. Chen[a,b,c,1,3], Lars Stangenberg[b], Elena Aikawa[b], Elisenda Rodriguez[b], Shumei Qiu[d], Michael A. Moskowitz[c,d], and Ralph Weissleder[a,b,c]

[a]Center for Systems Biology, [b]Center for Molecular Imaging Research, [d]Stroke and Neurovascular Regulation Laboratory, and [c]Department of Radiology, Massachusetts General Hospital, Harvard Medical School, CNY-149, 13th Street, Charlestown, MA 02129

Edited by Gerald D. Fischbach, The Simons Foundation, New York, NY, and approved October 14, 2008 (received for review April 24, 2008)

Inflammation can extend ischemic brain injury and adversely affect outcome in experimental animal models. A key difficulty in translating animal studies to humans is the lack of a definitive method to confirm and track inflammation in the brain in vivo. Myeloperoxidase (MPO), a key inflammatory enzyme secreted by activated neutrophils and macrophages/microglia, can generate highly reactive oxygen species to cause additional damage in cerebral ischemia. We report here that a functional, enzyme-activatable MRI agent can accurately track the oxidative activity of MPO noninvasively in stroke in living animals. We found that MPO is widely distributed in ischemic tissues, correlates positively with infarct size, and is detected even 3 weeks postinfarction. The peak level of MPO activity, determined by activation of the MPO-sensing agent in vivo and confirmed by MPO activity and quantitative RT-PCR assays, occurred on day 3 after ischemia. Both neutrophils and macrophages/microglia contribute to secrete MPO in the ischemic brain, although neutrophils peak earlier (days 1–3) whereas macrophages/microglia are most abundant later (days 3–7). In contrast to the conventional MRI agent diethylenetriamine-pentatacetate gadolinium, which reports blood–brain barrier disruption, MPO imaging is able to additionally track MPO activity and confirm inflammation on the molecular level in vivo, information that was previously only possible to obtain on ex vivo brain sections and impossible to assess in living human patients. Our findings could allow efficient noninvasive serial screening of therapies targeting inflammation and the use of MPO imaging as an imaging biomarker to risk-stratify patients.

inflammation | ischemia | molecular imaging | MRI | brain

Cerebral ischemia induces a complex cascade of biochemical and molecular changes, including inflammatory reactions and production of reactive oxygen species that can contribute to stroke progression. It has been shown that stroke patients with systemic inflammation exhibit poorer outcomes (1, 2). Although antiinflammatory therapy decreases infarct size and improves neurological sequelae in experimental animal models of stroke (3), human trials with antineutrophil therapy have not shown a clear benefit. This discrepancy is likely because experimental stroke is relatively homogeneous concerning size, territory, and etiology, and consequently inflammation is consistently elicited. However, human stroke is extremely heterogeneous (4), with different size and vascular territories involving different mechanisms. Therefore, there is a need to develop better inflammatory animal models and carefully select animals and individuals afflicted with stroke with a significant inflammatory component for antiinflammatory therapy and trials.

Inflammation in stroke has been traditionally identified on histopathology as neutrophil infiltration, which correlates positively with ischemic damage (5). Myeloperoxidase (MPO) is the most abundant component in azurophilic granules in neutrophils and has often been used as a histopathological marker for neutrophils (6). It is also expressed in the myeloid line, especially in monocytes and macrophages/microglia. MPO interacts with hydrogen peroxide to generate highly reactive species including hypochlorite (OCl^-) and radicalized oxygen species (O_2^-, $ONOO^-$). MPO-mediated radicalization of molecules induces apoptosis (7) and nitro-tyrosination of proteins (8). Therefore, MPO is a key component of inflammation and has been shown to play a major role in animal models of stroke in the posthypoxic inflammatory response (9, 10). In human cerebral ischemia, certain MPO genotypes are associated with increased brain infarct size and poorer functional outcome (11). In addition, serum MPO levels are elevated in human stroke patients compared with normal subjects (12) and can predict future stroke and vasculopathic events in Fabry disease (13). Additionally, serum MPO levels are elevated in other cardiovascular diseases in humans, including myocardial infarction (14), congestive heart failure (15), and peripheral vascular disease (16). Therefore, whereas inflammation is a complex cascade of events involving different types of cells and molecules, MPO could be used as a biomarker for inflammation, and a noninvasive method to identify MPO activity in the ischemic brain could allow clinicians to identify those patients that would most likely benefit from antiinflammatory therapy.

In this study, we report a noninvasive MRI method to detect MPO activity and thus biologically relevant active inflammation. We demonstrate that the imaging results correlate with infarct size, histopathological findings, and quantitative biochemical MPO assays. We show that noninvasive detection of active inflammation in experimental stroke is feasible. This work sets the stage in the future for the use of this molecular imaging technology to select and risk stratify the vulnerable stroke patients who can benefit from antiinflammatory therapy and to monitor treatment changes from antiinflammatory therapy.

Results

Activation of the MPO-Sensing Agent Results in Higher Enhancement Levels than Conventional Imaging with Diethylenetriamine-Pentatacetate Gadolinium (DTPA-Gd) in Stroke and Is Specific to MPO. In the presence of MPO the 5-hydroxytryptamide moiety of bis-5-hydroxytryptamide-diethylenetriamine-pentatacetate gadolinium (MPO-Gd) is oxidized and radicalized. The radicalized MPO-Gd molecule can react with another radicalized MPO-Gd molecule to form a polymer of up to 5 subunits. The activated agent can also bind to proteins, trapping the agent at the site of inflammation, further increasing its molecular weight, and leading to an additional increase in T_1-weighted signal (17) (Fig. 1*A*). Thus, prolonged

Author contributions: M.O.B., J.W.C., M.A.M., and R.W. designed research; M.O.B., J.W.C., L.S., E.A., E.R., and S.Q. performed research; L.S., E.R., and S.Q. contributed new reagents/analytic tools; M.O.B., J.W.C., L.S., E.A., M.A.M., and R.W. analyzed data; and M.O.B., J.W.C., M.A.M., and R.W. wrote the paper.

The authors declare no conflict of interest.

This article is a PNAS Direct Submission.

[1]M.O.B. and J.W.C. contributed equally to this work.

[2]Present address: Department of Neuroradiology, Klinikum Rechts der Isar, Technische Universität München, Ismaningerstrasse 22, 81675 Munich, Germany.

[3]To whom correspondence should be addressed. E-mail: chenjo@helix.mgh.harvard.edu.

This article contains supporting information online at www.pnas.org/cgi/content/full/0803945105/DCSupplemental.

www.pnas.org/cgi/doi/10.1073/pnas.0803945105

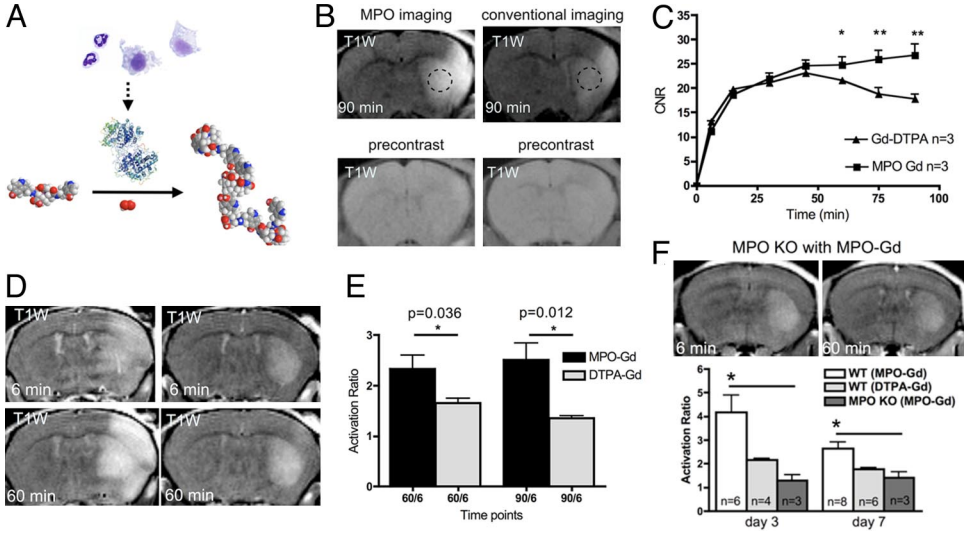

Fig. 1. MPO-sensing agent activation. (*A*) Mechanism of the MPO agent activation: MPO oxidizes the 5-hydroxytryptamide (5HT) moiety of MPO-Gd that leads to oligomerization and the activated agent can further bind to proteins. This results in a large increase in longitudinal relaxation rate (R_1) and prolonged enhancement at sites of increased MPO activity. (*B*) Representative example at 90 min of an animal imaged with the 2 agents, on days 7 (DTPA-Gd) and 8 (MPO-Gd). The oval indicates the area used for the image analysis. (*C*) MPO imaging results in higher CNRs than those of conventional imaging on delayed time points. Direct comparison of the 2 agents in the same animals imaged 1 day apart shows a 15% higher enhancement level of MPO-Gd at 60 min ($P = 0.013$) and 35% higher at 90 min after agent injection ($P = 0.001$). One animal was imaged with MPO-Gd first, and 2 animals were given DTPA-Gd first. (*D*) Representative images of the increased enhancement from MPO activation at 60 min compared with 6 min in 2 different animals, showing different degrees of MPO activation. (*E*) Activation ratios of MPO-Gd at 60 and 90 min demonstrate significantly higher CNRs than those of DTPA-Gd. *, $P < 0.05$; **, $P < 0.01$. (*F*) MPO imaging in MPO KO mice. Representative images of MPO imaging in MPO KO mice at 6 and 60 min after MPO-Gd administration (day 7), demonstrating no obvious increased enhancement at 60 min compared with the 6-min image. Activation ratios on days 3 and 7 after cerebral ischemia revealed statistically significant differences between MPO-Gd imaging of WT and MPO knockout mice and between MPO-Gd and DTPA-Gd imaging of the WT mice. No statistically significant difference was found between MPO-Gd imaging of MPO knockout mice and DTPA-Gd imaging of WT mice. These findings confirm specificity of MPO-Gd imaging.

enhancement can be detected for >60 min at sites of increased MPO activity. In contrast, the enhancement pattern of DTPA-Gd, the clinical gold standard for contrast enhanced brain imaging, is significantly different because the nonactivatable DTPA-Gd becomes diminished in contrast enhancement after 45 min in infarcted areas and is only 87% as hyperintense at 60 min ($P = 0.013$) and 65% at 90 min ($P = 0.001$) compared with MPO-Gd. (Fig. 1 *B* and *C*).

For the conventional DTPA-Gd agent, the degree of enhancement is a reflection of agent leakage across the compromised blood–brain barrier (BBB) in the injured tissues. However, for MPO-Gd, the enhancement is the result of both leakage across the BBB and enzyme-mediated activation. The difference in enhancement between MPO-Gd and DTPA-Gd is particularly striking on the delayed MR images (Fig. 1 *B–D*), indicating that these late images when compared with the early time points allow the detection of inflammatory foci. Therefore, to obtain a better assessment of MPO-mediated agent activation, we took the first postcontrast images as the baseline in which the enhancement was predominately from leakage and the 1-h delayed images to reflect both leakage and activation. Thus, the ratio of enhancement between these 2 sets of images better represents the degree of MPO-mediated activation and is more reflective of MPO activity (hereon referred to as activation ratio). This measure showed significantly higher ratios for the MPO-sensing agent compared with those for DTPA-Gd (Fig. 1*E*) at 60 and 90 min ($P = 0.036$ and 0.012, respectively).

To evaluate the specificity of MPO-Gd for MPO, we performed MPO-Gd imaging in MPO knockout mice on days 3 and 7 postischemia and compared with results from WT mice imaged with MPO-Gd and DTPA-Gd at the same time points postischemia (Fig. 1*F*). In MPO knockout mice, there was no evidence of MPO-Gd activation, because the activation ratios were similar to those of WT mice imaged with the conventional DTPA-Gd agent and significantly smaller compared with MPO-Gd imaging in WT mice. These results confirmed the specificity of MPO-Gd for MPO.

MRI Allows Serial Tracking of Inflammation Over Time in Stroke. Representative examples of MPO imaging are shown for 2 different animals with corresponding apparent diffusion coefficient (ADC) maps and T_2-weighted images to confirm the area of ischemia (Fig. 2 *A* and *B*). Quantitative contrast-to-noise ratio (CNR) analysis of the delayed images showed highest absolute enhancement levels at day 7 after infarction (Fig. 2*C*). As noted above, this enhancement is the result of both leakage and agent activation. The activation ratios instead peaked on day 3 and remained elevated on day 7, indicating that the highest activation of MPO-Gd occurred during this time period (Fig. 2*D*). There was still detectable activation on day 21 postischemia, underlining the long-term inflammatory tissue disturbance in the infarcted area (Fig. 2*D*). There was good correlation on each day ($R^2 = 0.84$) between the infarct volume and the absolute CNR, indicating that bigger strokes contained more MPO.

Activated Neutrophils and Macrophages Secrete 10 Times Higher Amounts of MPO than Their Nonactivated Counterparts. To test the MPO expressing capacity of neutrophils and macrophages, both cell types were isolated from the bone marrow of nondiseased animals. The cells were activated in vitro, and we compared the MPO activity levels of the activated cells to those from the nonactivated cells. We found that both stimulated macrophages and neutrophils secreted ≈10 times more MPO than the nonstimulated cell ($P = 0.043$ for neutrophils and $P = 0.044$ for macrophages). Furthermore, macrophages and neutrophils expressed similarly high amounts of MPO (Fig. 3*A*).

MPO Activity Assays and Quantitative RT-PCR (qRT-PCR) Correlate Well with MPO Imaging and Confirm That the Activation of the Probe Reflects MPO Expression. To confirm the presence of MPO in the ischemic brain, we performed Western blot analysis. We found

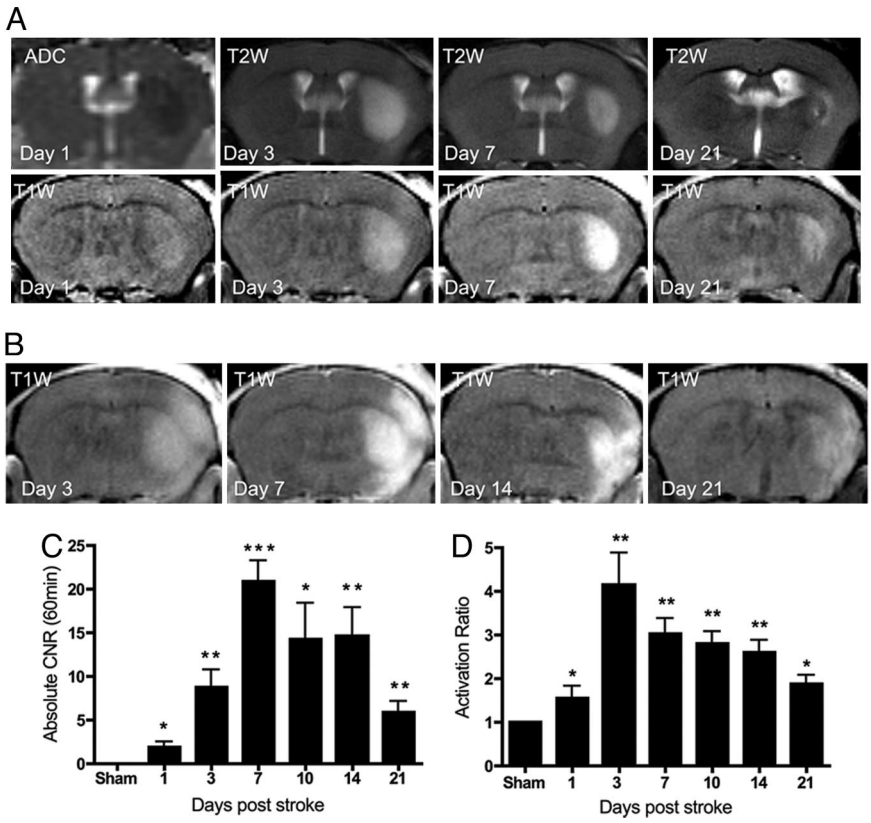

Fig. 2. MPO imaging allows tracking of inflammation in stroke in vivo over time. (*A*) (*Upper*) Infarct development over time is shown on ADC and T_2-weighted images. (*Lower*) Corresponding sections in the same mouse imaged with MPO-Gd (at 60 min after agent injection) show the enhancement evolution over time. (*B*) MPO imaging of a different mouse. (*C*) Quantitative analysis over 3 weeks after infarct demonstrates that the absolute CNR enhancement, which represents both BBB breakdown and MPO activation of the agent, peaks on day 7 ($P < 0.05$ on all days compared with the sham-operated animals). (*D*) Activation ratio of the MPO agent reveals that the highest MPO activity occurs on day 3 after stroke and remains elevated on day 21 ($P < 0.05$ on all days compared with the sham operated animals). *, $P < 0.05$; **, $P < 0.01$; ***, $P < 0.001$.

elevated MPO levels expressed in ischemic but not in sham-operated animals (Fig. 3*B*).

We also performed MPO activity assays to quantitatively track MPO activity over time and validate MRI results. We found that MPO activity of the ischemic hemisphere was significantly elevated compared with the sham-operated animals from days 1 to 14 ($P < 0.05$). The highest MPO activity levels were found between day 3 (3-fold up-regulation) and day 7 (2.5-fold up-regulation; Fig. 3*C*). The MPO activity assay mirrored the MPO imaging results and correlated with the absolute delayed CNR values ($R^2 = 0.65$) and MPO-Gd activation levels ($R^2 = 0.85$). Notably, the absolute CNR values correlated less well than the activation ratios, underscoring the validity of the analysis and that the latter measurement better reflects MPO activity. Similarly, qRT-PCR results showed the highest relative MPO mRNA expression levels in the ischemic hemisphere on day 3 (Fig. 3*D*; 2.7-fold up-regulation, $P < 0.01$). At

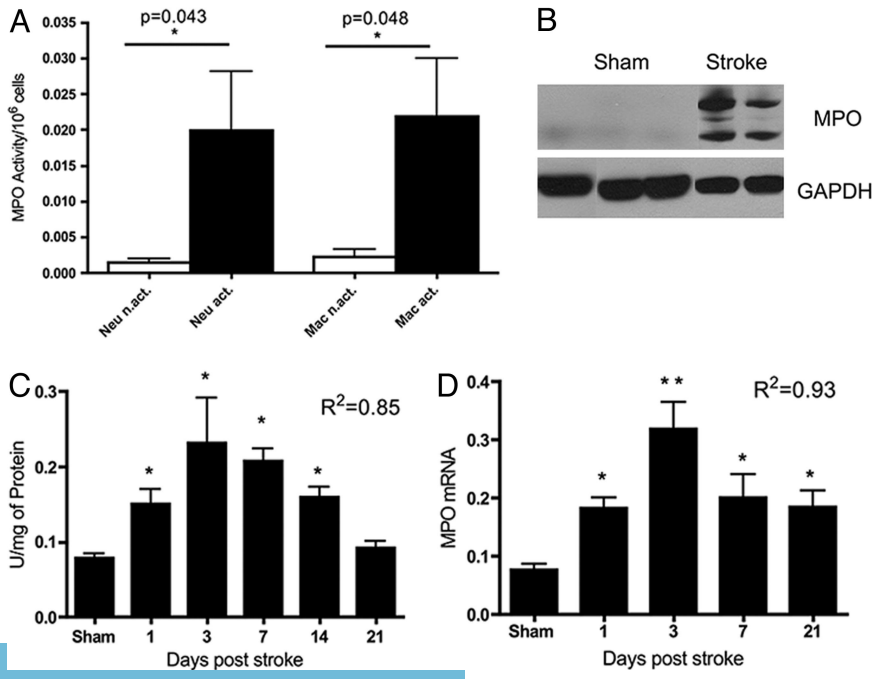

Fig. 3. Biochemical analyses corroborate MPO imaging findings. (*A*) MPO activity of activated macrophages/neutrophils (act. Mac/Neu) show that both express ≈10-fold higher MPO levels compared with the nonactivated cells (n.act. Mac/Neu) ($P = 0.044$ for macrophages and $P = 0.043$ for neutrophils). (*B*) Western blots confirm elevated MPO levels in the ischemic brain. Western blots detect high levels of the MPO precursor protein (92 kDa) and the MPO heavy chain (60 kDa) in the ischemic hemisphere, whereas only faint background levels of MPO exist in the sham-operated animals. GAPDH (38 kDa) is shown as a loading control. (*C*) MPO activity assays correlate with the MR imaging results. The MPO activity assays results confirm that the peak of MPO expression is at day 3 and shows significantly higher MPO expression ($P < 0.05$) compared with the sham-operated animals on all days except day 21. The MPO assay results correlate well with the activation ratio ($R^2 = 0.85$). (*D*) qRT-PCR for MPO mRNA confirms the activation ratio ($R^2 = 0.93$) and the enzyme activity assays ($R^2 = 0.83$). *, $P < 0.05$; **, $P < 0.01$.

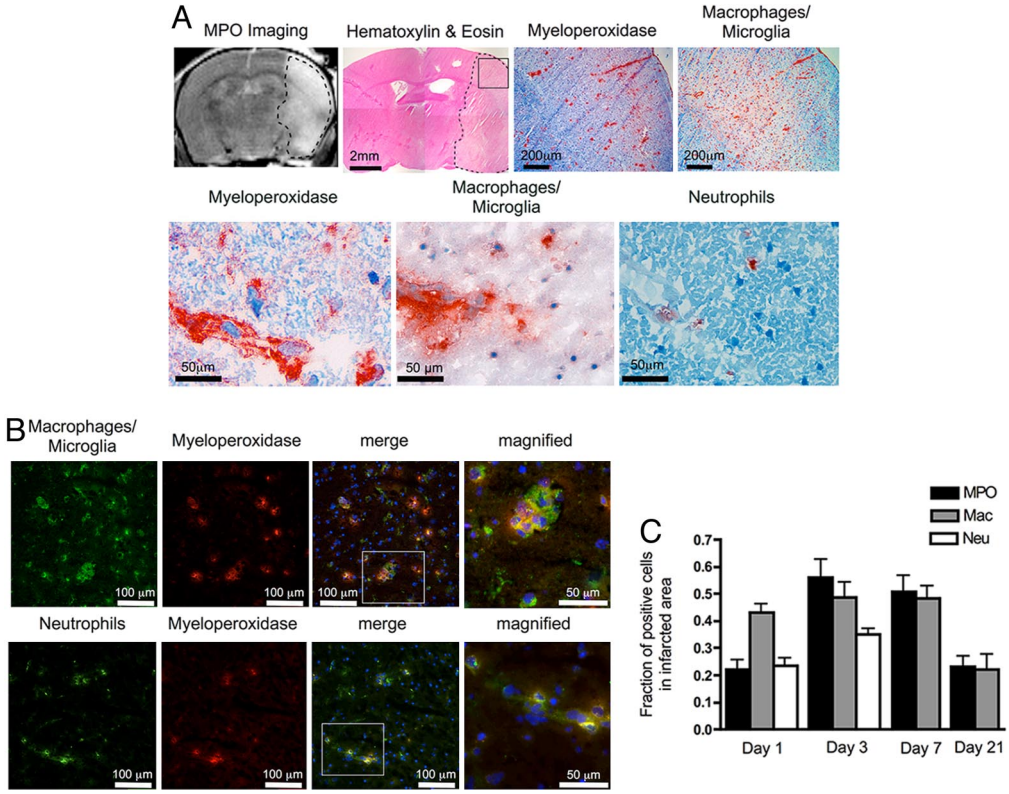

Fig. 4. Histopathological analyses correspond to MPO imaging findings. (*A*) MPO imaging on day 3 after infarction shows a large area of enhancement in the basal ganglia and cerebral cortex. The infarct appears as pale areas in the cortex and basal ganglia (H&E). The corresponding MPO immunostaining demonstrates diffuse MPO expression predominately from macrophages/microglia in the infarct. Lower row shows high-resolution images. (*B*) MPO is expressed by both neutrophils and macrophages (day 3). Double immunofluorescence staining of macrophages (green) and MPO (red) (*Upper*) and neutrophils (green) and MPO (red) (*Lower*) show both cell types as a source of MPO (day 3). Nuclei are counterstained with DAPI (blue). (*C*) Quantification of the inflammatory cell influx over time. Neutrophils were detected on days 1 and 3, whereas macrophages/microglia were observed over the entire investigated period of 3 weeks, with the highest levels on days 3 and 7. MPO-positive cells were detected throughout the entire investigated period and exhibited the highest levels on days 3 and 7, similar to the MPO imaging and biochemical results.

days 1, 7, and 21, MPO mRNA expression was also significantly higher than in the sham-operated animals ($P < 0.05$). qRT-PCR results further showed excellent correlation with the activation ratios of the MPO-imaging results ($R^2 = 0.93$), which again was better than the correlation to the absolute CNR ($R^2 = 0.52$). These results corroborate the accuracy of the MPO in vivo imaging technology in tracking MPO levels.

MPO Is Expressed Throughout the Infarcted Area by both Neutrophils and Macrophages. To further analyze the cellular pathophysiology we performed histopathological analysis, which matched well with MRI concerning lesion size and infarcted area. MPO could be detected throughout the entire infarct (Fig. 4*A*). No discrete distribution pattern of MPO could be delineated in our study, which confirmed our imaging finding of relatively diffuse and homogeneous MPO agent enhancement within the infarct. An infiltration of both neutrophils and macrophages/microglia into the infarct region was detected (Fig. 4*A*) that was not present in the nonischemic hemisphere (data not shown). Neutrophils were fewer than macrophages in absolute numbers and only seen on days 1–3. Macrophages/microglia and MPO-positive cells were abundantly present in the infarct throughout the investigated time period with the highest levels on days 3 and 7 (Fig. 4 *A* and *C*). Double immunofluorescence microscopy for MPO and macrophages/microglia and MPO and neutrophils revealed that both neutrophils and macrophages/microglia are the sources for MPO in this stroke model (Fig. 4*B*). Notably, a 1-mm-sized lesion, barely visible on T_2-weighted images, was still detected on MPO imaging 3 weeks postinfarction. The lesion correlated well with histopathological analysis, which showed macrophages/microglia as the source of MPO at this late time point (Fig. 4*C* and [supporting information (SI) Fig. S1].

Discussion

In the present study, we demonstrate that MPO activity can be noninvasively tracked and imaged serially in living animals with cerebral ischemia. We found that MPO, a key enzyme secreted in the inflammatory response to tissue injury, is widely distributed in the ischemic tissues, and correlated positively with infarct size. The peak level of MPO activity, determined by activation of the MPO-sensing agent in vivo and confirmed by MPO activity assays and qRT-PCR analyses, occurred on day 3 after ischemia in our model, similar to previous ex vivo findings (5). Both neutrophils and macrophages/microglia contribute to secrete MPO in the ischemic brain, although neutrophils peak earlier (days 1–3), whereas macrophages/microglia are most abundant later (days 3–7). In contrast to the conventional, nonspecific agent DTPA-Gd, which reports BBB disruption (18), MPO imaging is able to additionally report MPO activity and confirm inflammation on the molecular level in vivo, information that was previously only possible to obtain on ex vivo brain sections and impossible to be assessed in living human patients.

MPO imaging harnesses the power of enzymatic amplification. In the presence of MPO, the small molecule MPO-sensing agent, MPO-Gd, can serve as a substrate for MPO and become radicalized. The activated, radicalized parent molecules can combine into oligomers, which are more effective at shortening proton T_1, thus increasing the image intensity on T_1-weighted MR imaging. This process leads to increased sensitivity to MPO activity. In addition, the activated agents can bind to proteins, causing prolonged retention of the activated agents at sites of increased MPO activity (17), which allows confirmation of MPO activity on delayed images. We have confirmed the specificity of MPO-Gd for MPO in MPO knockout mice in this stroke model (Fig. 1*F*) and in a mouse model of myocardial infarction (19). These properties allow highly sensitive and specific detection and confirmation of MPO expression in vivo.

Inflammation can extend ischemic injury (20) to adversely affect stroke outcome (21) and may provide new therapeutic targets to treat patients outside of the narrow thrombolysis window of 3–6 h. For example, in a recent study it was shown that the administration of the drug AM-36, a Na^+ channel blocker and an antioxidant,

could reduce MPO activity and improve functional outcome after stroke in mouse models (22). Furthermore, the long-lasting increased MPO expression >3 weeks found in our study suggests that inflammation plays a role in cerebral ischemia well into the late subacute stage. Thus, by tracking MPO activity noninvasively, MPO imaging can serve as an imaging biomarker for inflammation. The current lack of definitive human data to support effective antiinflammatory therapy thus far likely reflects a dearth of developed drugs in relevant inflammatory animal models to target different inflammatory factors in stroke and our inability to select patients who may benefit from antiinflammatory treatment. It is possible that MPO imaging could help risk stratify patients and select those who would most likely benefit from antiinflammatory treatment. MPO imaging could also be used in experimental and preclinical studies to screen and assess treatment efficacy of novel therapeutic drugs and to reduce the number of animals needed for ex vivo evaluations.

Recently, several studies have reported the use of magnetic nanoparticles to identify inflammatory regions in stroke (4, 23–25). However, magnetic nanoparticles detect only macrophages/microglia, which are thought to be less associated with acute inflammatory damage in stroke and do not correlate with infarct size, whereas neutrophil infiltration and MPO correlated well with infarct size (5). Furthermore, it has been shown that some of the magnetic nanoparticles may be trapped by thrombi instead of taken up by macrophages, further limiting its use (26). However, although MPO imaging can accurately report and track inflammation, a potential limitation of our study is that MPO imaging does not discriminate between MPO secreted from neutrophils or macrophages/microglia. To identify the relative contributions from these inflammatory cell types in vivo, a combination of MPO and macrophage imaging would likely be useful. Another limitation of our study, inherent in many animal models of stroke, is in the use of young healthy mice, which lack the various comorbidities seen in human stroke patients. It should also be noted that MPO activity obtained from tissue extracts is likely affected by proteases that are present in inflamed tissues, which can lead to degradation of the MPO protein, resulting in lower activities compared with imaging and qRT-PCR techniques. Inhibiting the proteases (e.g., with sodium azide) would also result in a dampening of MPO activity. This effect is likely the reason that imaging, qRT-PCR, and histopathological analyses were consistent with the presence of elevated MPO level on day 21, whereas MPO activity assay for day 21 was only slightly elevated but not statistically different from that of sham animals. Because we performed the biochemical analyses on homogenized hemispheres, which included unaffected tissue, the values obtained likely slightly underestimate the levels of MPO protein and expression.

MPO imaging is also applicable to many other cardiovascular, neurovascular, and neurodegenerative inflammatory processes in which elevated MPO expression has been described (27). For example, we have recently shown increased diagnostic sensitivity and specificity of MPO imaging compared with conventional imaging in mouse models of multiple sclerosis (28) and myocardial infarction (19), and studies on vasculitis and atherosclerosis are ongoing. We are actively investigating the toxicity of MPO-Gd, and preliminary data revealed that MPO-Gd is not taken up by cells such as activated macrophages, thus would not cause DNA damage, and has no significant cytotoxic effect up to at least 5 mM (unpublished data). MPO imaging thus represents a promising technology to determine the expression of the key enzyme MPO noninvasively over time in many clinically important inflammatory diseases, and future studies using this approach could result in new potent therapies against inflammatory damage in stroke.

Methods

Animal Model of Stroke. The protocol for animal experiments was approved by the institutional animal care committee. Animals were purchased from Jackson Laboratory. Right-sided cerebral ischemia was induced in C57/black6 mice (n = 40) weighing 23.8 ± 2.7g by occluding the right middle cerebral artery temporarily for 30 min using a thread occlusion model as described (29). Sham-operated animals (n = 6) were used as controls in which the internal carotid artery was isolated but no suture was inserted. Right-sided cerebral ischemia was also induced in MPO knockout mice (n = 3). Animals with intracranial hemorrhage were excluded from the study (n = 5) because hemorrhage is a potential confounding factor in preventing accurate infarct volume assessment and can skew the inflammatory response in the hemorrhagic areas, given that hemorrhage itself could elicit a strong inflammatory response (30) and obscure inflammation arising from cerebral ischemia.

Imaging Agents. The MPO-sensitive MR agent DTPA-Gd, MPO-Gd was synthesized as described (31). DTPA-Gd (Magnevist) was purchased from Berlex Laboratories.

Imaging. MR imaging was performed on a 7 T Bruker Pharmascan MRI scanner. Precontrast and postcontrast T_1-weighted images [time to repeat (TR) = 800, time to echo (TE) = 13; 4 signals acquired, acquisition time of 6 min 57 s, matrix size 256 × 192, field of view 2.5 × 2.5 cm, slice thickness 0.8 mm, 18 sections acquired] were obtained after the i.v. administration of 0.3 mmol/kg of either the MPO-sensing agent MPO-Gd or the conventional, nonselective agent DTPA-Gd. Postcontrast imaging was obtained at 6, 15, 30, 45, 60, 75, and 90 min sequentially for 60 or 90 min after contrast administration. In addition, to more directly compare both agents we imaged the same animals (n = 3) with both agents. These animals were imaged 1 day apart (days 7 and 8) to ascertain that the previous agent has been cleared from the animal and to avoid cross-contamination of the agents. To minimize differences resulting from lesion evolution between imaging sessions, we administered 1 animal with MPO-Gd first and the other 2 animals with DTPA-Gd first.

Histopathological Analyses. ***Immunohistochemical analyses.*** Animals were killed by compressed carbon dioxide, and the brains were removed and washed in distilled water. The cerebellum was separated from the cerebrum and not used for further analysis because it was not infarcted in the animals. The hemispheres of the cerebrum were separated and frozen over dry ice in isopentane in the embedding media OCT. Samples were stored at −80 °C before further processing of the tissue. Five-micrometer coronal sections of fresh frozen tissues were examined for the presence of MPO (rabbit polyclonal antibody; AbCam), macrophages/microglia (mac-3; BD Biosciences), and neutrophils (Santa Cruz). The avidin-biotin peroxidase method was used. The reaction was visualized with the 3,3′-diaminobenzidine method (Sigma). All sections were counterstained with hematoxylin. Tissue sections from sham-operated animals were used as controls. Hematoxylin–eosin staining was also performed to study the overall morphology. Images were captured with a digital camera (Nikon DXM 1200-F).

Double immunofluorescence microscopy. To show colocalization of MPO with macrophages/microglia or neutrophils, we performed double-labeling fluorescence microscopy. The same antibodies were used as for histopathology. Secondary antibodies were detected with streptavidin conjugated with Texas red (MPO) or streptavidin coupled to FITC (macrophages/microglia, neutrophils) (both 1:100; Amersham). Counterstaining for nuclei was performed with DAPI. An avidin/biotin blocking kit (Vector Laboratories) was used to prevent cross-reaction of the antibodies. A Nikon 80i microscope was used for image taking.

Quantification of immunohistochemistry. Macrophage/microglia, neutrophil, and MPO staining were quantified by manually counting the immunoreactive cells in 5 predetermined cerebral regions (3 within the parietal cortex, 2 within the basal ganglia) of the ischemic hemisphere in 400× high-power fields across different stereotactic levels. A mean was calculated for each region, and the ratio of immunoreactive cells per total number of cells was used to account for cell loss in the stroke area (n = 3).

Western Blot Analysis. To confirm the presence of MPO in the stroke area, ischemic brain hemispheres were homogenized and extracted in 1% cetyltrimethylammonium bromide (Sigma-Aldrich) in 100 mM KPO_4 buffer, pH 7.0. The resultant suspensions were sonicated for 30 s and then underwent 3 cycles of freeze–thaw in liquid nitrogen. Subsequently, the suspensions were centrifuged at 16,000 × g for 15 min and the supernatant used for protein quantification analysis with the bicinchoninic acid kit (Pierce). Western blots were performed by using a monoclonal rabbit anti-mouse MPO antibody (Upstate) at 1:1,000 dilution, and a rabbit anti-mouse polyclonal GAPDH antibody (Rockland) at 1:5,000 dilution using chemiluminescence detection. Thirty micrograms of protein from the samples was loaded, and GAPDH was used as a loading control.

Isolation of Monocytes/Macrophages and Neutrophils. Naive monocytes/macrophages and neutrophils were extracted from the bone marrow (n = 6) and

purified by a 75%, 65%, and 55% step gradient centrifugation of Percoll (Sigma-Aldrich) as described (32). Cells were washed twice in HBSS, counted with a hemocytometer using trypan blue exclusion as viability marker, and incubated for 2 h at 37 °C with 5% CO_2 in 0.5 mL of DMEM (Mediatech) with or without 1 μL of 4 mM of phorbol 12-myristate-13-acetate (Sigma-Aldrich) to stimulate cells to secrete MPO. After the incubation cells were spun at 1,500 $\times$ *g* for 5 min, and the supernatant was used for MPO activity quantifications.

MPO Activity Assay with Guaiacol. To quantify MPO activity in isolated monocytes/macrophages and neutrophils, we performed MPO activity assays (33), which test MPO activity against the substrate guaiacol on a UV/visible spectrometer (Varian Cary 50 Bio UV-Vis spectrometer) at 470 nm. The assay solution consists of 0.1 M phosphate buffer at pH 7, supplemented with 48 μL of guaiacol and 100 μL of 0.1 M H_2O_2. One-hundred microliters of cell supernatants was added to 500 μL of assay solution in a 600-μL cuvette. The units of activity were computed according to the following formula: activity = $(\Delta OD \times V_t \times 4)/(E \times \Delta t \times V_s)$, where ΔOD is change in absorbance, V_t is total volume, V_s is sample volume, E (extinction coefficient) = 26.6 mM^{-1}, and Δt is change in time. The resultant activity was normalized to 10^6 cells.

MPO Activity Assay with Tetramethylbenzidine (TMB). To measure the MPO activity in ischemic brain hemispheres and correlate the MPO activity to MPO imaging results we used the TMB assay (Sigma-Aldrich), which has a higher sensitivity than the guaiacol assay (34) and detects the oxidation of 3,5,3′,5′-TMB by MPO through a change in absorbance at 655 nm. Mice brains were prepared as described above for Western blot analyses. Fifty microliters of extracted protein was added to 950 μL of assay solution, and the change in absorbance was measured over 10 min. At least $n = 3$ was used for each time point and units of activity were calculated as with the guaiacol assay above, but with *E* (extinction coefficient) = 3.9×10^4 $M^{-1} \cdot s^{-1}$. Units of activity were normalized to 1 mg of protein.

qRT-PCR. Total RNA was isolated from the ischemic hemisphere and sham-operated control animals by using TRIzol (Invitrogen). Oligo(dT) primers were used to reversely transcribe mRNA into cDNA following the manufacturer's guidelines (StrataScript; Stratagene). qRT-PCR was performed on an ABI SDS 7000 system using ABgene QPCR Rox Mix and standard cycling conditions. The standard curve method was used to calculate cDNA content of samples. Every sample was run in triplicate, and 3 samples per time point were assessed. GAPDH (Applied Biosystems) was chosen as an internal calibrator. Primer sequences were generated by using PrimerExpress. MPO primers were: TTTGACAGCCTGCACGATGA (forward), GTCCCCTGCCAGAAAACAAG (reverse), and CACCAACCGCTCCGCCCG (probe).

Statistical Analysis. CNRs were computed for each region of interest (ROI) according to the formula: CNR = ((postcontrast ROI_{lesion} − postcontrast $ROI_{contralateral\ normal\ side}$)/$SD_{noise}$) − (precontrast ROI_{lesion} − precontrast$_{contralateral\ normal\ side}$)/$SD_{noise}$), where ROI_{lesion} is the ROI of the enhancing area in the basal ganglia (Fig. 1*B*). The basal ganglia was used for ROI analysis because it was consistently affected by the induced ischemia, whereas the cortex was not involved in all animals. For $ROI_{contralateral\ normal\ side}$ the ROI of the stroke side was mirrored to the noninfarcted hemisphere, and SD_{noise} is the standard deviation of noise measured from an ROI placed in an empty area of the image. CNRs were normalized where indicated by dividing each CNR by the highest CNR. Three imaging slices were analyzed and averaged. MPO-Gd activation was determined by computing the ratio $CNR_{60\ min}/CNR_{6\ min}$, because early enhancement (6 min after contrast agent injection) represents mostly leakage through BBB breakdown, whereas enhancement after 60 min comes mainly from MPO activation. The lesion volume was calculated by multiplying the lesion area of all infarcted slides measured on ADC maps (day 1–3) and T_2-weighted images (days 7–21) with the slice thickness. The resultant data were analyzed with the 1-tailed Student's *t* test with the null hypothesis that MPO imaging is not better at detecting inflammation than conventional DTPA-Gd and that MPO is not expressed in higher amounts in stroke animals compared with sham-operated animals. $P < 0.05$ was considered to be statistically significant. All statistical computations were performed with the statistical software package Prism 4.0c (GraphPad). All error bars indicate SEM.

ACKNOWLEDGMENTS. We thank Carlos Rangel, Claire Kaufman, Anne Yu, Jenny Chan, Vincent Lok, Todd Sponholtz, Yoshiko Iwamoto, and Ying Wei for experimental assistance and Peter Panizzi for helpful discussions. We acknowledge early contributions by Alexei Bogdanov and Manel Querol in developing MPO-Gd. M.O.B. was supported by the German National Academic Foundation and Boehringer Ingelheim Fonds. L.S. received support from the German Research Foundation. E.R. was supported by the Marie Curie Fellowship. This work was supported in part by National Institutes of Health Grants 5K08HL081170 (to J.W.C.), P50-NS10828-32 (to M.M.), and R24-CA92782 and R01-HL078641 (to R.W.).

1. McColl BW, Rothwell NJ, Allan SM (2007) Systemic inflammatory stimulus potentiates the acute phase and CXC chemokine responses to experimental stroke and exacerbates brain damage via interleukin-1- and neutrophil-dependent mechanisms. *J Neurosci* 27:4403–4412.
2. Elkind MS, Cheng J, Rundek T, Boden-Albala B, Sacco RL (2004) Leukocyte count predicts outcome after ischemic stroke: The Northern Manhattan Stroke Study. *J Stroke Cerebrovasc Dis* 13:220–227.
3. Nakamura T, *et al.* (2007) Pioglitazone exerts protective effects against stroke in stroke-prone spontaneously hypertensive rats, independently of blood pressure. *Stroke* 38:3016–3022.
4. Saleh A, *et al.* (2007) Iron oxide particle-enhanced MRI suggests variability of brain inflammation at early stages after ischemic stroke. *Stroke* 38:2733–2737.
5. Weston RM, Jones NM, Jarrott B, Callaway JK (2007) Inflammatory cell infiltration after endothelin-1-induced cerebral ischemia: Histochemical and myeloperoxidase correlation with temporal changes in brain injury. *J Cereb Blood Flow Metab* 27:100–114.
6. Rausch PG, Pryzwansky KB, Spitznagel JK (1978) Immunocytochemical identification of azurophilic and specific granule markers in the giant granules of Chediak-Higashi neutrophils. *N Engl J Med* 298:693–698.
7. Lo EH, Moskowitz MA, Jacobs TP (2005) Exciting, radical, suicidal: How brain cells die after stroke. *Stroke* 36:189–192.
8. Lau D, Baldus S (2006) Myeloperoxidase and its contributory role in inflammatory vascular disease. *Pharmacol Ther* 111:16–26.
9. Matsuo Y, *et al.* (1994) Correlation between myeloperoxidase-quantified neutrophil accumulation and ischemic brain injury in the rat. Effects of neutrophil depletion. *Stroke* 25:1469–1475.
10. Takizawa S, *et al.* (2002) Deficiency of myeloperoxidase increases infarct volume and nitrotyrosine formation in mouse brain. *J Cereb Blood Flow Metab* 22:50–54.
11. Hoy A, *et al.* (2003) Myeloperoxidase polymorphisms in brain infarction. Association with infarct size and functional outcome. *Atherosclerosis* 167:223–230.
12. Re G, *et al.* (1997) Plasma lipoperoxidative markers in ischaemic stroke suggest brain embolism. *Eur J Emerg Med* 4:5–9.
13. Kaneski CR, Moore DF, Ries M, Zirzow GC, Schiffmann R (2006) Myeloperoxidase predicts risk of vasculopathic events in hemizygous males with Fabry disease. *Neurology* 67:2045–2047.
14. Mocatta TJ, *et al.* (2007) Plasma concentrations of myeloperoxidase predict mortality after myocardial infarction. *J Am College Cardiol* 49:1993–2000.
15. Tang WH, *et al.* (2006) Plasma myeloperoxidase levels in patients with chronic heart failure. *Am J Cardiol* 98:796–799.
16. Brevetti G, *et al.* (2007) Myeloperoxidase, but not C-reactive protein, predicts cardiovascular risk in peripheral arterial disease. *Eur Heart J* 29:224–230.
17. Chen JW, Querol Sans M, Bogdanov A, Jr, Weissleder R (2006) Imaging of myeloperoxidase in mice by using novel amplifiable paramagnetic substrates. *Radiology* 240:473–481.
18. Knight RA, *et al.* (2005) Quantitation and localization of blood-to-brain influx by magnetic resonance imaging and quantitative autoradiography in a model of transient focal ischemia. *Magn Reson Med* 54:813–821.
19. Nahrendorf M, *et al.* (2008) An activatable MR imaging agent reports myeloperoxidase activity in healing infarcts and detects attenuation of ischemia-reperfusion injury by atorvastatin noninvasively. *Circulation* 117:1153–1160.
20. Hossmann KA (2006) Pathophysiology and therapy of experimental stroke. *Cell Mol Neurobiol* 26:1057–1083.
21. Saeed SA, Shad KF, Saleem T, Javed F, Khan MU (2007) Some new prospects in the understanding of the molecular basis of the pathogenesis of stroke. *Exp Brain Res* 182:1–10.
22. Weston RM, Jarrott B, Ishizuka Y, Callaway JK (2006) AM-36 modulates the neutrophil inflammatory response and reduces breakdown of the blood–brain barrier after endothelin-1 induced focal brain ischaemia. *Br J Pharmacol* 149:712–723.
23. Wiart M, *et al.* (2007) MRI monitoring of neuroinflammation in mouse focal ischemia. *Stroke* 38:131–137.
24. Nighoghossian N, *et al.* (2007) Inflammatory response after ischemic stroke: A USPIO-enhanced MRI study in patients. *Stroke* 38:303–307.
25. Jander S, Schroeter M, Saleh A (2007) Imaging inflammation in acute brain ischemia. *Stroke* 38:642–645.
26. Bendszus M, Kleinschnitz C, Stoll G (2007) Iron-enhanced MRI in ischemic stroke: Intravascular trapping versus cellular inflammation. *Stroke* 38:e12; author reply (2007) 38:e13.
27. Hoy A, Leininger-Muller B, Kutter D, Siest G, Visvikis S (2002) Growing significance of myeloperoxidase in noninfectious diseases. *Clin Chem Lab Med* 40:2–8.
28. Chen JW, Breckwoldt MO, Aikawa E, Chiang G, Weissleder R (2008) Myeloperoxidase-targeted imaging of active inflammatory lesions in murine experimental autoimmune encephalomyelitis. *Brain* 131:1123–1133.
29. Huang Z, *et al.* (1994) Effects of cerebral ischemia in mice deficient in neuronal nitric oxide synthase. *Science* 265:1883–1885.
30. Gong C, Hoff JT, Keep RF (2000) Acute inflammatory reaction following experimental intracerebral hemorrhage in rat. *Brain Res* 871:57–65.
31. Querol M, Chen JW, Weissleder R, Bogdanov A, Jr (2005) DTPA-bisamide-based MR sensor agents for peroxidase imaging. *Org Lett* 7:1719–1722.
32. Boxio R, Bossenmeyer-Pourie C, Steinckwich N, Dournon C, Nusse O (2004) Mouse bone marrow contains large numbers of functionally competent neutrophils. *J Leukocyte Biol* 75:604–611.
33. Klebanoff SJ, Waltersdorph AM, Rosen H (1984) Antimicrobial activity of myeloperoxidase. *Methods Enzymol* 105:399–403.
34. Marquez LA, Dunford HB (1997) Mechanism of the oxidation of 3,5,3′,5′-tetramethylbenzidine by myeloperoxidase determined by transient- and steady-state kinetics. *Biochemistry* 36:9349–9355.